Non-Markovian behavior of ultrafast coherent ionization dynamics in a crystal exposed to a seeded free-electron-laser pulse

A. Brand,[*] B. Kaiser, A. Vagov, and V. M. Axt

Institut für Theoretische Physik III, Universität Bayreuth, 95447 Bayreuth, Germany

U. Pietsch

Universität Siegen, 57068 Siegen, Germany

We investigate the ionization dynamics of a crystal structure driven by ultrafast coherent x-ray pulses of moderate to high intensities for excitations where dipole-allowed, single-photon ionization dominates. Using a simple model of the crystal, we demonstrate that quantum coherences may already play an important role at moderate pulse intensities, leading to qualitatively novel features which cannot be described by rate equations. In particular, the ionization may exhibit a minimum as a function of the pulse duration, where the ionization drops to almost zero, although during the pulse a noticeable fraction of the electrons is promoted to unbound states. For higher intensities, the qualitative deviations between the coherent quantum-mechanical treatment and the rate description is even more pronounced. In particular, due to the presence of quantum-mechanical coherences, the full theory predicts, even for the single-photon transitions to a continuum of free-electron states, a Rabi-type behavior similar to what is known for two-level systems.

I. INTRODUCTION

The availability of large-scale free-electron-laser (FEL) facilities all over the world, e.g., Free electron LASer (FLASH) in Germany [1], Linac Coherent Light Source (LCLS) in California [2], SPring-8 Angstrom Compact free-electron LAser (SACLA) in Japan [3], and FERMI in Italy [4], as high-brilliance ultrafast xuv and x-ray sources provides the tools needed to explore the electron motion on a time scale of femtoseconds. Triggered by these advances, experimental and theoretical developments have been pushed forward to study phenomena induced by ultrashort light-matter interaction mediated by FEL pulses [5–10].

So far, recent experiments could often be well described by rate equations [11,12] which involve a Markov approximation. This approximation neglects memory effects reflecting the electronic coherences that are built up by the pulse. One reason for the success of rate descriptions is the presence of fast relaxation mechanisms on a time scale of a few femtoseconds that suppress coherent electron dynamics [13,14]. Examples are the Auger decay mediated by the electron-electron inter-action and the fluorescence resulting from the electron-light coupling. Furthermore, the creation of the pulses in FELs by self-amplified stimulated emission (SASE) introduces strong statistical fluctuations [15], which may mask signatures of coherent or non-Markovian dynamics. Even measuring the pulse profile of ultrafast x-ray pulses is a demanding task, which has been achieved only recently [16]. Although recent theoretical studies of the atomic ionization dynamics indicate that non-Markovian dynamics may become of importance at high intensities [17,18], the experimental observation of coherent phenomena in the ionization dynamics is still a chal-lenging task. Nevertheless, recent experiments [19] confirmed a theoretical prediction [20] that the multipeak structure due to coherent Rabi oscillations between two resonantly driven

bound states can still be visible as an additional broadening of the Auger electron spectrum after the statistical averaging introduced by SASE excitation.

A major obstacle for these experiments has been the sufficient energetic isolation of the resonantly driven transi-tion [19,21]. This problem is particularly severe for unseeded pulses that, e.g., at LCLS exhibit a bandwidth of 0.5%–1.0% of the photon energy [10]. With up-to-date seeding techniques, pulse durations below 1 fs [22,23] and a high stability [4,24,25] are within reach. Nearly transform-limited femtosecond pulses that become available with these techniques provide a band-width of only a few electronvolts, which is an order of magnitude smaller than the bandwidth of typical unseeded pulses, thus paving the way toward direct investigations of coherent signatures in the ionization dynamics.

In this paper, we shall discuss coherent phenomena in the ionization dynamics evoked by strong, coherent, ultrashort x-ray laser pulses in a crystal. We focus mostly on scenarios where slow free electrons are created. Although we consider a situation where direct single-photon ionization is dominant and thus the conditions are favorable for the application of rate equations, we find qualitative deviations from the coherent quantum-mechanical treatment already at moderate intensities. At high intensities, the time evolution strongly resembles Rabi oscillations, even though we are not dealing with the classical Rabi scenario where two discrete states are resonantly coupled by a laser. Instead, the radiation couples a narrow band of initially occupied orbitals with the states in the continuum just above the ionization threshold. In particular, our studies show that the coherent Rabi-type dynamics may strongly reduce the ionization. Rate equations completely fail to account for these dynamical features.

II. THEORY

A. Equation of motion

A widely used approach to describe the ionization from core shells in many-atom systems, such as macromolecules

---

[*]andre.brand@uni-bayreuth.de

or solids, is to calculate ionization rates for the constituent atoms, thereby treating the atoms as independent [26,27]. In a crystal the leading order correction to this picture of noninteracting atoms is to replace the atomic by a lattice periodic potential V_{periodic}. Whether or not further corrections, such as many-electron effects resulting from electron-electron interactions, are of importance depends on the specific system and on the physical quantity to be studied. For example, it is well known that Coulombic correlations play a decisive role for the enhanced double ionization of helium in strong infrared fields [28–30]. On the other hand, calculations of the total ionization dynamics via a resonant intermediate state for a similar system with and without accounting for the electron-electron interaction agreed qualitatively for most of the predicted dependencies, i.e., the differences were restricted to quantitative changes that, although noticeable, did not affect the overall physical picture [18]. Here we present a model study where we concentrate on the short time dynamics of the ionization process itself, accounting for the lattice periodic potential but neglecting any further many-particle effects. Our main interest is the dynamics that takes place during the pulse, i.e., in the fully coherent regime, and we focus on ionization processes that generate slow electrons that within 1 fs do hardly reach the neighboring atom. Thus impact ionization, which in a first step requires the acceleration of an electron that then ionizes a neighboring atom, will be of minor importance. The model Hamiltonian that describes the interaction of the crystal with an external coherent laser reads

$$H = \sum_j \frac{1}{2m}\left(\frac{\hbar}{i}\vec{\nabla}_j + e\vec{A}(\vec{x}_j,t)\right)^2 + V_{\text{periodic}}(\vec{x}_j), \quad (1)$$

where $\vec{A}$ is the vector potential of the radiation field and m is the free-electron mass. This Hamiltonian can be split according to

$$H = H_0 + H_{\text{field}} \quad (2)$$

into a field-free part H_0 and the field interaction part H_{field}. Diagonalizing H_0 yields the band structure $\epsilon_{n\vec{k}}$ and the corresponding Bloch states $|\psi_{n\vec{k}\sigma}\rangle$ with band index n, wave vector $\vec{k}$, and spin σ, respectively.

Since we intend to discuss coherent phenomena, we consider seeded FEL pulses that are well described by a classical field. In addition to disregarding the quantum nature of the laser field, we also assume a single well-characterized envelope free of random fluctuations. We note that for SASE pulses the situation would be different, despite the high photon numbers of $>10^{11}$ [31], which are in favor of a classical description. Due to the lack of coherence, which results from the chaotic phases that occur in SASE pulses, photoionization cross sections are expected to undergo strong fluctuations near resonances [32].

In order to describe the dynamics of our model system, we set up equations of motion for the reduced density matrix:

$$\varrho_{nm}(\vec{k},\vec{k}') := \langle c_{n\vec{k}\sigma}^\dagger c_{m\vec{k}'\sigma}\rangle, \quad (3)$$

where $c_{n\vec{k}\sigma}^\dagger$ and $c_{n\vec{k}\sigma}$ are the creation and annihilation operators of an electron in a Bloch state $|\psi_{n\vec{k}\sigma}\rangle$. The spin indices are omitted on the left-hand side of Eq. (3), since we shall discuss only situations where all density matrices are spin independent

for all times. The Heisenberg equations for the operators $c_{n\vec{k}\sigma}^\dagger$ and $c_{n\vec{k}\sigma}$ generate a closed set of equations of motion for $\varrho_{nm}(\vec{k},\vec{k}')$ because the Hamiltonian, Eq. (2), comprises only single-particle contributions. We assume that initially the system is in its ground state, which implies that initially $\varrho_{nm}(\vec{k},\vec{k}')$ is diagonal. The corresponding equations of motion are given by

$$i\hbar\frac{d}{dt}\varrho_{nm}(\vec{k},\vec{k}')$$

$$= (\epsilon_{m\vec{k}} - \epsilon_{n\vec{k}'})\varrho_{nm}(\vec{k},\vec{k}') + \sum_{\vec{k}'',\tilde{n}}[W_{m\tilde{n}}(\vec{k}',\vec{k}'')\varrho_{n\tilde{n}}(\vec{k},\vec{k}'')$$

$$- W_{n\tilde{n}}^*(\vec{k},\vec{k}'')\varrho_{\tilde{n}m}(\vec{k}'',\vec{k}')], \quad (4)$$

where $W_{nn'}(\vec{k},\vec{k}') := \langle\psi_{n\vec{k}\sigma}|H_{\text{field}}|\psi_{n'\vec{k}'\sigma}\rangle$.

B. Specification of the crystal model

Since the goal of our work is to demonstrate the importance of coherent effects and not the study of a given specific crystal, we consider a simple Kronig-Penney potential in a single spatial dimension that is typically a good starting point for a qualitative description of solid-state properties [33]. In this model the periodic potential is defined as

$$V_{\text{periodic}}(x) = \begin{cases} -V_0, & \text{if } x \in \bigcup_{n\in\mathbb{Z}}[-a+nd,a+nd] \\ 0, & \text{else} \end{cases}.$$

$$(5)$$

Note that the zero of energy is put at the top of the core potential, such that states with positive energies describe electrons that are still within the solid but typically have enough energy to leave the crystal once they reach the boundaries [34]. In this sense we shall refer to these electrons as *free electrons*. The occupation of free-electron states at long times after the pulse that drives the excitation is gone can be regarded as a measure of the total ionization induced by the pulse. Secondary processes, e.g., electron-electron collisions and Auger decay, are likely to generate further free electrons at longer time scales, depending on the distribution of free electrons induced by the laser pulse.

One-dimensional soft core potentials have been used successfully to model the ionization dynamics of atomic systems like helium and lithium [17,18,35], as well as of solids where the Mathieu or the Kronig-Penney potential have been used [33]. The Kronig-Penney model guarantees that the corresponding low-energy Bloch states are strongly localized near the core positions such that the electron density decays exponentially between the cores. A similar behavior is known for $3d$ Coulomb systems.

For numerical simulations, we choose the core-core distance $d = 5$ a.u. and define the Kronig-Penney model by the parameters for the width of an individual rectangular potential barrier of $a = 1$ a.u. and its depth $V_0 = 6$ a.u. The resulting band structure is shown in Fig. 1(a), where k is measured in units of the length of the reciprocal lattice vector of minimal length $g = \frac{2\pi}{d}$. As expected, the lowest bands have a rather small width [hardly seen on the scale of Fig. 1(a)]. The electron density corresponding to these Bloch waves is strongly localized at the cores. This is illustrated in Fig. 1(a) for the example of the $k = 0$ state of the lowest band ($n_b = 1$), where the real-space wave
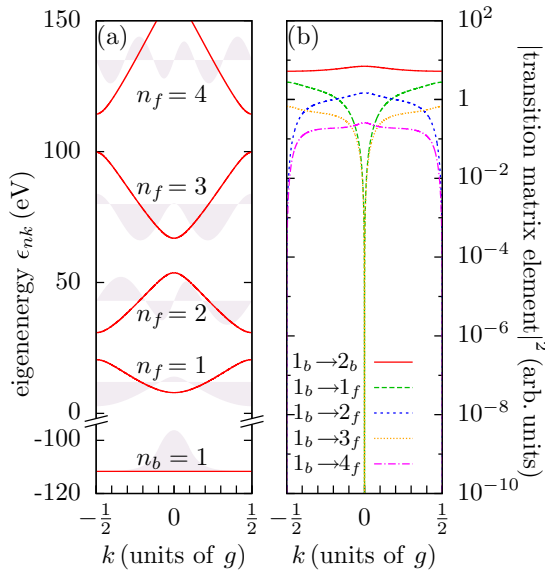
FIG. 1. (Color online) (a) Band structure of the Kronig-Penney model for the parameters chosen in Sec. II B, where ϵ_{nk} denotes the energy of a state in the n_bth bound band with wave vector k or the n_fth free band, respectively. The eigenstates at $k=0$ in real space, i.e., $\psi_{nk=0}(x)$, of the respective band are outlined in the background. (b) Transition matrix elements for $n_b \to n_f$ transitions. As an example, for a bound-bound transition the results for the $1_b \to 2_b$ transition are also shown.

function is displayed in the background of the corresponding band over the range of a single-lattice cell. With our choice of zero energy, a negative energy implies that the electron does not have sufficient energy to escape from the core potential. We shall refer to such bands as *bound bands* and label them with band indices $n_b \in \mathbb{N}$.

For bands with positive energies, the character of the orbitals changes and now the electron density between the cores is significant, as expected for free electrons. This can be seen in Fig. 1(a), where the $k=0$ orbitals are plotted. Bands with positive energies corresponding to free electrons will be labeled with band indices $n_f \in \mathbb{N}$ in the following.

Note that the electron spectrum has gaps also for positive energies, even far above the ionization threshold. This behavior is expected for any periodic $1d$ potential, because for electron energies much higher than the depth of the core potential, the electrons can be reliably described in the model of quasifree particles in a periodic potential. For this limiting case it is known from standard textbook discussions that in each band at the zone boundary a gap opens proportional to the coefficients $V_{\pm g}$ of the period potential lattice vector g with minimal length. For a $3d$ potential this analysis applies as well to any given direction in reciprocal space. However, as the energy at the zone boundary depends on the direction, there might not be gaps in the density of states anymore. But also in this case typically van Hove singularities appear. The resulting enhanced density of states resembles the situation just above such a gap in $1d$. Thus we expect our $1d$ model to capture essential properties of realistic systems at least qualitatively. In particular, the feature that the interaction with the periodic lattice leaves a trace also in the density of free-electron states is not an artefact of the $1d$ model.

We assume that initially the band with lowest energy is fully occupied while all other bands are empty. Our numerical studies presented below concentrate on excitations where the laser frequency is tuned in resonance to transitions from the lowest band ($n_b = 1$) to one of the free-electron bands $n_f \in \{1,2\}$. For such excitation conditions, the transition from the lowest band to the free-electron states dominates the ionization in real systems, even when energetically higher bands are initially occupied. We shall further assume that the wave vector of the laser can be neglected, which implies that the transitions between different bands appear at fixed k.

In order to get an overview of the relative importance of different transitions, we have plotted in Fig. 1(b) momentum matrix elements for several transitions starting from the lowest band. These matrix elements determine the corresponding photoionization cross sections. The largest matrix elements are found for transitions between bound bands and exhibit only a marginal k dependence [cf., e.g, the $1_b \to 2_b$ transition in Fig. 1(b)]. In contrast, the matrix elements of transitions from a bound to a free-electron band depend strongly on k. This k dependence is to a large extent dictated by the symmetry of the lattice periodic functions $u_{n,k}(x)$ in the Bloch solutions that are either even or odd at $k=0$. For transitions between bound states, these functions depend on k only weakly and thus the resulting transition matrix elements exhibit only a weak k dependence. For transitions from bound to free-electron bands, where the corresponding $u_{n,k}$ functions have the same parity at $k=0$, the selection rules lead to a suppression of the transition matrix elements in a finite range at around $k=0$.

C. Connection to rate descriptions

The ionization via a dipole-allowed direct single-photon process which connects states in continua fulfills all criteria that are commonly considered to justify the applicability of a rate equation description. One of the goals of the present paper is to show that even under these favorable conditions, rate approaches come to their limits when the pulses are very strong and/or the pulse duration is short. In order to make explicit the connection between the full Schrödinger theory and the rate equation limit, and for later reference, we shall shortly summarize the main steps needed to derive rate equations starting from our equations for density matrices. We restrict the discussion to the $1d$ version of the general equations of Sec. II A and use a vector potential which depends only on time,

$$A(t) = A_0(t)\cos(\omega_0 t), \quad (6)$$

i.e., we neglect the spatial variation of the amplitude $\vec{A}_0$, which for typical FEL pulses is localized in the range of micrometers [31] and assume crystals that are smaller than the laser focus. With these assumptions Eq. (4) simplifies to

$$i\hbar\frac{d}{dt}\varrho_{nm} = (\epsilon_m - \epsilon_n)\varrho_{nm} + \sum_j (W_{mj}\varrho_{nj} - W_{nj}^*\varrho_{jm}), \quad (7)$$

where the matrix elements are $W_{nj} \to W_{nj}(k) := \frac{e}{m}A(t)\langle\psi_{nk\sigma}|\hat{p}|\psi_{jk\sigma}\rangle$ and $\varrho_{nm} := \langle c_{nk\sigma}^\dagger c_{mk\sigma}\rangle$. Equation (7)

exhibits only a parametric dependence on the Bloch wave vector k that is omitted in the notations. Note that the term involving A^2 disappears from the equation as a consequence of the spatial homogeneity of the field.

Rate equations for occupation numbers of quantum states, i.e., for the diagonal elements of the density matrix ϱ_{nn}, are obtained from the equations of motion for the density matrix by eliminating the off-diagonal elements. Writing Eq. (7) for the $n = m$ elements of ϱ_{nm},

$$\frac{d}{dt}\varrho_{nn} = \sum_j g_{jn}(t), \quad g_{jn}(t) := \frac{2}{\hbar}\text{Im}(W_{nj}\varrho_{nj}), \quad (8)$$

we can identify a generation rate $g_{jn}(t)$ for the occupation of state n which accounts for transitions between states with quantum numbers $j \leftrightarrow n$. The summation can be restricted to $j \neq n$ because $g_{jj}(t) = \text{Im}(W_{jj}\varrho_{jj}) = 0$. By integrating Eq. (7) for $n \neq m$ with an initial condition $\lim_{t \to -\infty} \varrho_{nm}(t) = 0$, i.e., initially only the diagonal elements are nonzero, we obtain

$$\varrho_{nm}(t) = \frac{1}{i\hbar}\int_{-\infty}^t dt' e^{i\omega_{nm}(t-t')}\sum_j [W_{mj}(t')\varrho_{nj}(t') - W_{nj}^*(t')\varrho_{jm}(t')], \quad (9)$$

where we have introduced the transition frequency $\omega_{nm} := \frac{1}{\hbar}(\epsilon_n - \epsilon_m)$. In the next step, we neglect contributions from off-diagonal elements of the reduced density matrix on the right-hand side of Eq. (9). This can be justified by both a perturbation and a time-scale argument. The perturbation argument rests upon an iterative approach with a diagonal initial state, while the time-scale argument makes use of $\varrho_{nm}(t) \propto e^{i\omega_{nm}t}$, where ω_{nm} is comparable to the laser frequency and is much faster than the ionization dynamics, i.e., the time scale of the occupation numbers.

Inserting the so-simplified Eq. (9) into Eq. (8) and introducing an auxiliary quantity $\tilde{W}_{nj}(t) := e^{i\omega_{nj}t}W_{nj}(t)$, one obtains for the generation rate

$$g_{jn}^{\text{res}}(t) = \frac{2}{\hbar^2}\text{Re}\left[\tilde{W}_{nj}(t)\int_{-\infty}^t dt' \tilde{W}_{jn}(t')(\varrho_{jj}(t') - \varrho_{nn}(t'))\right]. \quad (10)$$

The generation rate $g_{jn}^{\text{res}}(t)$ will therefore be noticeably distinct from zero on resonance when $\tilde{W}_{nj}(t)$ has a contribution in time that does not average out. Despite the fact that only occupation numbers are present, the equation of motion, Eq. (8), with the generation rate, Eq. (10), is not a rate equation in the conventional sense, since it contains a memory. Furthermore, it comprises fast oscillations of the laser field that give rise to off-resonant driving terms. These off-resonant parts can be eliminated by the replacement

$$\tilde{W}_{nj}(t) \to \frac{e}{2m}A_0(t)e^{i\delta\omega_{nj}t}\langle\psi_{nk\sigma}|\hat{p}|\psi_{jk\sigma}\rangle,$$

$$\text{where } \delta\omega_{nj} := \begin{cases} \omega_{nj} - \omega_0 & \text{for} \quad \omega_{nj} > 0 \\ \omega_{nj} + \omega_0 & \text{for} \quad \omega_{nj} < 0 \end{cases}, \quad (11)$$

which is known as the rotating wave approximation (RWA). In the following, we will refer to Eq. (10) including the RWA as a *resonant approximation*. Thus the resonant approximation neglects off-resonant contributions while still keeping the

memory. Conventional rate equations are obtained from the resonant approximation by neglecting the memory, i.e., by performing the Markov approximation. In Ref. [36] the Markov limit for the generation rate has been explicitly worked out for a Gaussian pulse, $A_0(t) = \bar{A}_0 \exp(-\frac{t^2}{2\tau_0})$, resulting in the *Markovian generation rate*,

$$g_{jn}^{\text{Markov}}(t) = (\varrho_{jj}(t) - \varrho_{nn}(t))\frac{2\pi}{\hbar^2}\left|W_{nj}^{(0)}(t)\right|^2 S(\delta\omega_{nj}), \quad (12)$$

where $W_{nj}^{(0)}(t) = \frac{e}{2m}A_0(t)\langle\psi_{nk\sigma}|\hat{p}|\psi_{jk\sigma}\rangle$ and $S(\omega) = \frac{\tau_0}{\sqrt{2\pi}}\exp(-\tau_0^2\omega^2)$ comprises the spectral properties of the excitation. Note that $S(\omega)$ approaches a δ distribution for long pulses in the limit $\tau_0 \to \infty$, which represents the energy conservation in a single-photon absorption. Therefore Fermi's golden rule is recovered as a special case of Eq. (12).

III. RESULTS AND DISCUSSION

A. Ionization dynamics at moderate intensities

In this section we shall present numerical results for the ionization dynamics at not too high intensities. To be specific, we have adjusted the intensities for the calculations in this section such that according to the usual rate equation estimates, the resulting depletion of the lowest band stays below 30%. Our main interest here is the dependence of the ionization probability on the pulse length, which turns out to be nontrivial. From our numerical solution of the equations of motion we extract the total occupation of free-electron states. The long time limit of this quantity can be regarded as an estimate for the ionization probability. All calculations have been carried out for Gaussian pulses.

In Fig. 2(a) we have plotted the results of simulations for different pulse durations ($\tau :=$ full width half maximum of the intensity), keeping fixed the photon number per pulse, i.e., the time integral over the intensity. The laser frequency has been adjusted in resonance to the transition $1_b \to 1_f$ at $k = \frac{1}{4}g$, i.e., above the single-photon ionization threshold for transitions between the $n_b = 1$ and $n_f = 1$ bands. As the time scale of the ionization process is mainly dictated by the pulse length, we have chosen τ as the unit of time in Fig. 2 in order to facilitate the comparison of results for different pulse durations. Also shown in Fig. 2(a) are results of calculations using the resonant approximation [cf. Eqs. (10) and (11)]. It turns out that for moderate intensities the results of the resonant approximation and the full theory coincide for practically all cases. For short pulses we see deviations in the form of steplike structures that are superimposed on the rising curves in the full calculation which are missing in the resonant approximation. These structures can be attributed to the RWA contributions that are left out in the resonant approximation. The overall conclusion from this comparison is that for the conditions studied here it is justified to keep only resonant contributions to the dynamics.

Figure 2(a) demonstrates a pronounced dependence of the free-electron occupation dynamics on the pulse duration. For short pulses below $\tau \approx 0.2$ fs, the free-state occupation rises monotonically with time and the final occupation rises with rising pulse duration. For longer τ the behavior changes qualitatively. Now the time traces exhibit a maximum and
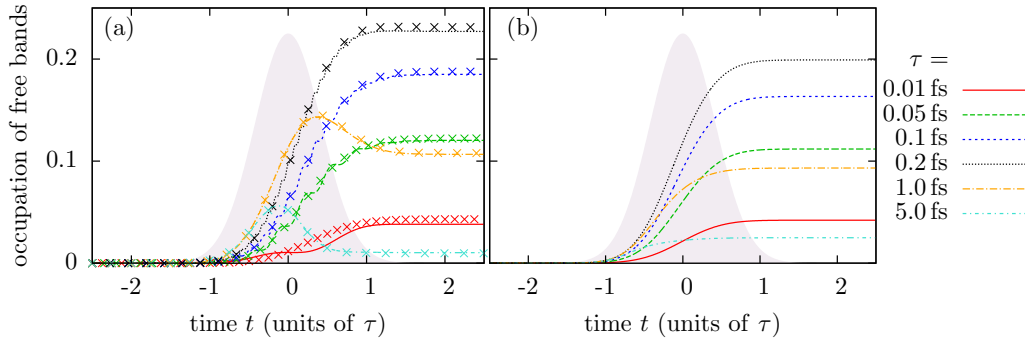
FIG. 2. (Color online) Ionization dynamics for a photon energy $\hbar\omega_0 = 125$ eV tuned to the resonance energy of the transition $1_b \rightarrow 1_f$ at $k = \frac{1}{4}g$ for different pulse lengths τ of Gaussian pulses, keeping the number of total photons fixed. τ is the FWHM of the intensity as indicated in the legend. The temporal envelope of the laser intensity is sketched in the background. Note that because the unit of time is the pulse lengths in these plots, the pulse envelopes are the same for all τ apart from the scaling of the amplitude. Plotted is a single representative envelope. The panels refer to different levels of theory described in the text: (a) full Schrödinger theory [Eq. (7), lines] and resonant approximation [Eq. (10), crosses], and (b) Markovian approximation Eq. (12).

the final occupation drops with rising τ. In order to better understand the origin of these dependencies, it is instructive to compare these findings with corresponding results from rate equations with the Markovian rates Eq. (12) displayed in Fig. 2(b). Here the final value also initially rises with increasing τ until at $\tau \approx 0.2$ fs a maximum is reached. For larger τ a monotonic decrease with growing τ is found. Furthermore, in the Markovian limit all time traces rise monotonically with time. The rise and fall of the final value that appears in both the full theory and the Markovian limit can be understood as follows: for the shortest pulses considered here, the pulse spectrum is so broad that a noticeable part of the excitation is in the transparent region outside all bands and thus gives only marginal contributions to the ionization. Increasing the pulse length makes the spectrum narrower and consequently, a larger portion of the supplied intensity leads to ionization. Once most of the spectrum is in the band region, a further increase of the pulse duration concentrates the excitation closer to the central frequency of the pulse which is near the middle of the $n_f = 1$ band. Thus the excitation directly at the band edges, where the density of states is enhanced, is reduced and therefore a drop of the ionization with rising τ has to be expected from this mechanism. The nonmonotonic behavior of the real-time traces, however, cannot be explained using rate equations. For a description of this feature, it is important to account for the memory that represents the influence of the phase-sensitive off-diagonal elements of the density matrix, i.e., the coherences. Although we are dealing here with transitions between continuous band states, the influence of the coherences is to some extent analogous to the well-known results for a laser-driven, two-level system where the occupation of the upper state varies in an oscillatory fashion with the pulse area, which rises with τ when the time-integrated intensity is kept fixed. This coherent mechanism is obviously superimposed to the nonmonotonic τ dependence of the final value that is also present when the ionization is modeled as an incoherent process by rates that connect only occupations which do not depend on quantum-mechanical phases.

As mentioned before, in current discussions of the ionization dynamics of many-atom systems, different approaches

are being used. In particular, instead of the Markovian rates [Eq. (12)] that are derived starting from a crystal model, the ionization can be accounted for by rates for the constituent atoms. Furthermore, for situations where the excitation is made by pulses that are not Fourier limited, it has been suggested to use rates that are averaged over the pulse spectrum [32]. Note that this procedure is not the same as using rates that explicitly depend on the spectral properties of the pulse, as, e.g., in the case of the Markovian rates [Eq. (12)]. It is thus illustrative to also compare the curves in Fig. 2 with the outcomes of other rate equation approaches. However, as this discussion is not the main target of the present paper, we present corresponding results in the Appendix and mention only in passing that for the conditions studied here the Markovian rates of Eq. (12) give better agreement with the full Schrödinger theory than other rate-based descriptions.

Most current experiments are not able to resolve the time traces shown in Fig. 2, as usually only the total ionization is recorded, which should be proportional to the long time value of the free-state occupation. The latter is plotted in Fig. 3 as a function of the pulse duration τ for all levels of the
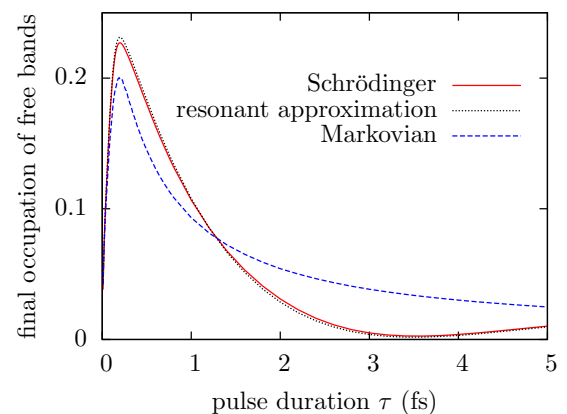
FIG. 3. (Color online) Final values of the free-electron occupations after the pulse for conditions as in Fig. 2, where the total photon number is kept constant and the pulse duration of Gaussian pulses with FWHM τ is varied.

theory that have been discussed in connection with Fig. 2. For short pulses a similar ionization is predicted for all levels of the theory. After passing the maximum at about $\tau \approx 0.2$ fs, both the Markovian and the Schrödinger theory predict a steep drop in ionization with increasing τ. For the Markovian case this drop is monotonic, while in the full quantum-mechanical calculation a minimal ionization is found for $\tau \approx 3.5$ fs, where the final value of the free-state occupation is close to zero. For large τ the Markovian and the full quantum-mechanical curves approach the same value. For long pulses the dynamics of the occupations slows down and thus going over to the Markov limit starting from the memory integral Eq. (10) is more and more justified. Consequently, the deviation of the Markovian from the full treatment vanishes. The difference between the full theory and the Markovian approximation is essentially the neglect of the memory in the latter case, which represents the coherences. In real systems the coherences can be suppressed, e.g., when phase relaxation processes that are not accounted for in our model become important. In such a case a complete treatment, which includes also the phase relaxation, should be well approximated by the Markovian limit.

It may at first sight appear counterintuitive that for 0.2 fs $\lesssim \tau \lesssim 3.5$ fs the ionization increases when τ decreases, because theoretical as well as experimental studies for atomic and molecular systems showed a suppression of radiation damage for short pulses [13,26,37,38] as soon as the pulse duration becomes short enough to be comparable to the decay time of the dominant relaxation process. However, our analysis applies to the short time dynamics in the coherent regime where the above-mentioned relaxation mechanisms are not yet important. Furthermore, it should be stressed once again that unlike many other studies, we are dealing here with Fourier-limited pulses for which the pulse length is correlated with the spectral width of the excitation. In such a case the drop of the ionization with increasing pulse duration is to a large extent related to the corresponding changes of the spectral properties of the excitation. Indeed, the fact that at $\tau \approx 3.5$ fs the free carrier occupation drops to almost zero implies that in this case the system was first excited and then practically completely deexcited by the incoming x-ray pulse. Therefore all secondary processes that usually follow the initial ionization and eventually destroy the crystal, such as impact ionization, for example, will not take place as the system is essentially back in its initial state after the pulse. Of course, the transitions induced by the laser pulse are the source of secondary emission. Thus the only secondary process that will occur is the interaction of the emitted photons with the crystal, which, however, will be much weaker than the interaction with the strong primary pulse. All together, the net effect of the excitation is that a secondary signal is emitted while the crystal after the pulse is essentially in its initial state, although during the pulse the system is driven far away from equilibrium. Comparing the Markovian calculations with the full theory yields insights about the role of coherences that are disregarded in the Markovian approach. We learn that phase relaxation processes, which destroy the coherences, inhibit the return of the system to its ground state, which is indicated by the minimum close to zero in the final excited-state occupation at $\tau \approx 3.5$ fs. A major relaxation mechanism not included in

our model is Auger recombination, which contributes to both phase and energy relaxation. Energy relaxation times due to Auger and other processes of the order of $\tau_E \approx 10$ fs have been reported, e.g., for L-shell excitations of solid-state silicon corresponding to a binding energy of around 100 eV, and the core-hole lifetime turns out to be approximately 19 fs [39]. For heavier elements and/or the K-shell, the relaxation is typically faster. An energy relaxation time τ_E sets an upper limit for the phase relaxation time of $\tau_{\mathrm{ph}} \geqslant 2\tau_E$. For τ_E of the order of 10 fs, the energy relaxation due to the Auger processes should not be a major influence for the dynamics during pulses with durations below $\tau = 3.5$ fs. With increasing τ the Auger relaxation will, of course, increase the final excited-state occupation. Consequently, the minimum seen in Fig. 3 is expected to be visible in the presence of Auger processes with $\tau_E \approx 10$ fs, provided the phase relaxation time is not too short.

B. Rabi cycling

This section is devoted to studies of the ionization dynamics at elevated intensities. Again, we keep the total photon number fixed, but at a value that is increased by a factor of 100 compared to the calculations presented before. Figure 4(a) displays corresponding time traces calculated using different levels of the theory for a fixed pulse duration τ. As an example we have chosen $\tau = 1$ fs, which for a Fourier-limited pulse corresponds to a spread of the pulse energy of ≈ 1.8 eV (FWHM), which is feasible for the new FEL sources with seeded pulses [cf. Sec. I]. The central frequency is chosen the same as in the previous section, such that the excitation is in resonance for transitions from the initially occupied band $n_b = 1$ to the free-electron band $n_f = 1$ at $k = \frac{1}{4}g$. As in the case of lower intensities, the Markovian rate approach leads to a monotonic rise of the free-state occupation. In sharp contrast, the full theory now
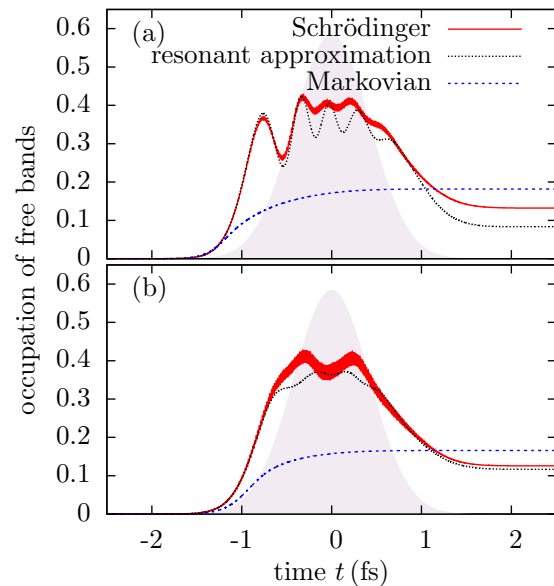
FIG. 4. (Color online) Ionization dynamics for $\tau = 1$ fs and a 100 times higher intensity than used in Fig. 2 for different central frequencies: (a) $\hbar\omega_0 = 125$ eV, i.e., tuned to the resonance of $1_b \rightarrow 1_f$ at $k = \frac{1}{4}g$, and (b) $\hbar\omega_0 = 120$ eV, i.e., tuned to the resonance of $1_b \rightarrow 1_f$ at $k = 0$.

predicts deeply modulated oscillations of the free-electron occupation that are not seen at lower intensities and are also absent in the rate equation results. Thus, even though we are dealing here with direct dipole-allowed transitions between continuous bands, we find Rabi-like dynamics similar to driven two-level systems. Obviously, at higher intensities coherences gain in importance. The results also demonstrate noticeable deviations of the resonant approximation from the full theory, indicating that off-resonant channels are no longer negligible at higher intensities, in accordance with previous findings for atomic systems [18]. Rabi cycling has been discussed before as a mechanism for suppressing the ionization probability in atomic systems that are excited via a resonantly coupled discrete intermediate state [40,41]. Our results demonstrate that also for crystals excited by direct single-photon processes, a substantial reduction of the ionization is possible.

The Rabi-type behavior is in our case a truly collective phenomenon in which many states of the resonantly coupled bands participate in a common nonlinear dynamics. Since important parameters like the density of states and the transition matrix elements vary noticeably within the bands, it can be expected that the resulting time traces change when the excitation is centered at different positions in the band. This is illustrated in Fig. 4(b), where we show results of calculations with the same parameters as in Fig. 4(a), but now for a central laser frequency in resonance with transitions to the lower band edge of the $n_f = 1$ band. The Markov theory predicts for an excitation at the band edge a slower rise of the excited-state occupation, as for a laser frequency tuned to transitions in the middle of the band. This reflects the fact that transitions to the $n_f = 1$ band with low k values are suppressed, because here the dipole matrix element at $k = 0$ vanishes due to selection rules [cf. Fig. 1(b)]. But overall, the Markov results for excitation at the band edge and in the middle of the band are similar. In particular, in both cases a monotonic rise is found and also the final values at long times are of similar order. In contrast, by comparing the results of the full Schrödinger theory for these two excitation conditions, we find large qualitative differences. For an excitation at the band edge, the modulation of the time-dependent excited-state occupation is much less pronounced, which can be attributed mainly to the strong k dependence of the dipole moments near $k = 0$ seen in Fig. 1(b). As the Rabi frequency for a resonantly driven transition is proportional to the transition matrix element, we are now essentially dealing with an ensemble of Rabi oscillations with a large spread in Rabi frequencies. The strong oscillatory modulations of the time traces are practically gone because of the destructive interference of the Rabi oscillations within this effective ensemble. Despite the suppression of the oscillations, the absolute values reached by the excited-state occupation are of similar magnitude for the two excitation conditions considered here. Obviously, the reduction of the dipole strength near the band edge is largely compensated by the enhanced density of states in this region. Finally, it is worthwhile to note that also for the case of near-band-edge excitations of the $n_f = 1$ band, a strong and qualitative difference between the full theory and the Markovian rate limit is found. While the latter predicts a monotonic rise as usual, in the full quantum-mechanical treatment we find a much steeper
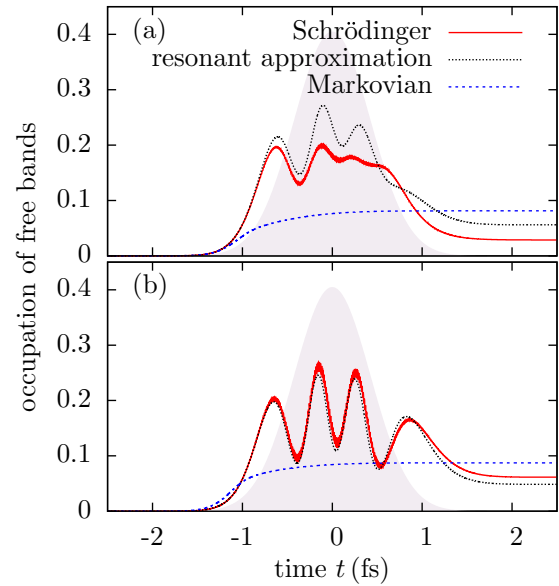
FIG. 5. (Color online) Ionization dynamics for $\tau = 1$ fs and a 100 times higher intensity than used in Fig. 2 for different central frequencies: (a) $\hbar\omega_0 = 153$ eV, i.e., tuned to the resonance of $1_b \rightarrow 2_f$ at $k = \frac{1}{4}g$, and (b) $\hbar\omega_0 = 165$ eV, i.e., tuned to the resonance of $1_b \rightarrow 2_f$ at $k = 0$.

rise followed by a weakly modulated plateau with a subsequent steep decrease, which eventually leads to a final value below the Markovian result.

Further insights into what determines the visibility of Rabi-type oscillations in transitions to free bands in a solid-state model can be obtained by comparing excitations from the $n_b = 1$ to the $n_f = 2$ band at $k = \frac{1}{4}g$ and $k = 0$, which is done in Fig. 5. Apart from switching the central frequency, all other parameters are the same as in Fig. 4. For a laser tuned in resonance with transitions to the $k = \frac{1}{4}g$ states in the $n_f = 2$ band [cf. Fig. 5(a)], in the Schrödinger theory a deep initial modulation is followed by several weaker oscillations, resulting in an overall behavior similar to that observed for the transitions to the $k = \frac{1}{4}g$ states in the $n_f = 1$ band. Obviously, the increased bandwidth of the second free band has only little influence on the Rabi-type dynamics. The errors caused by using the resonant approximation, however, turn out to be larger than in the corresponding case in the $n_f = 1$ band. Now, already during the first Rabi cycle, noticeable deviations to the Schrödinger theory results occur. Tuning the laser frequency in resonance with transitions to the $k = 0$ states of the $n_f = 2$ band [cf. Fig. 5(b)] results in a series of deeply modulated Rabi flops. For these excitation conditions the visibility of Rabi oscillations is enhanced due to a combination of three effects: (i) the dipole matrix elements near $k = 0$ depend only weakly on k for transitions to the $n_f = 2$ band; (ii) the density of states is peaked near $k = 0$, resulting in a large contribution to the excited-state occupation from a narrow region in the band; and (iii) for excitations near $k = 0$ the velocity of the excited free electrons is rather low and thus essentially no electrons can leave the region of their atoms before they are returned to their initial states in the course of a Rabi cycle. The comparison with calculations based on the resonant approximation reveals

for these excitation conditions an excellent agreement with the full theory, indicating that, as might have been expected, the visibility of band-Rabi oscillations is highest when the resonant transitions clearly dominate the dynamics.

IV. CONCLUSIONS

Using a simple model for a crystal, we have performed simulations of the ionization dynamics after the exposition of the crystal to a short and intense x-ray laser pulse. We have considered excitation conditions where direct allowed single-photon band-to-band absorption should be the dominant ionization channel, i.e., a situation favorable for applying the Markov approximation where the ionization is described by rate equations. In the short coherent pulse regime of pulse durations $0.2\,\text{fs} \lesssim \tau \lesssim 3.5\,\text{fs}$ and for moderate intensities, we find that the ionization drops with rising τ. A comparison between the Markovian result and the Schrödinger theory reveals that in this regime the total ionization can be noticeably reduced when the coherences that are disregarded in the Markov limit are not lost in dephasing processes. In the full treatment a minimal ionization close to zero occurs for $\tau \approx 3.5\,\text{fs}$, while the Markovian rate equations predict a monotonic decrease on a higher level.

At moderate intensities over a wide range of parameters, good qualitative agreement is found between the Markovian and the full quantum-mechanical theory, although already in this case rate equations are not able to explain the nonmonotonic time dependence of the free-state occupation that is found for some pulse durations in the full theory. However, this changes dramatically at higher intensities. While the Markovian theory still predicts a monotonic rise of the free-state occupation for all pulse lengths, the full theory exhibits qualitative new features. In particular, we find for band-to-band transitions Rabi-like oscillations that represent a collective behavior where a continuum of transitions participates. The oscillations disappear when the spread of Rabi frequencies of the involved transitions becomes too large. No matter whether or not oscillations are pronounced, we find in all cases a nonmonotonic time evolution of the free-electron occupation, in sharp contrast to the rate equation prediction. Moreover, the final value of the free-state occupation after the pulse, which is a measure for the ionization, can be controlled in a wide range by varying pulse properties such as pulse duration and intensity.

ACKNOWLEDGMENTS

APPENDIX: ATOMIC RATES

In this Appendix we shall compare the predictions for the ionization dynamics obtained from different rate equation approaches. Let us start by comparing the curves in Figs. 2(a) and 2(b) that were obtained for the full Schrödinger theory and the Markovian limit, respectively, with the result of a description where the ionization from the inner shell is

accounted for by a rate calculated for the constituent atoms. Here we use the standard golden rule formula for the atomic rate:

$$\Gamma_{\text{atomic}} := \frac{2\pi}{\hbar} D_{\text{atomic}}(\hbar\omega_{\text{ex}})|\langle\psi_i|H_{\text{field}}|\psi_f\rangle|^2, \qquad \text{(A1)}$$

where $\langle\psi_i|H_{\text{field}}|\psi_f\rangle$ denotes the transition matrix element between the atomic ground state and a free-electron state [42] with wave vector k, and $D_{\text{atomic}}(\hbar\omega_{\text{ex}})$ is the density of states of the atomic system at the excess energy $\hbar\omega_{\text{ex}}$, i.e., the energy by which the central laser energy $\hbar\omega_0$ exceeds the single-photon ionization threshold. For a meaningful comparison with our crystal model, we calculated the atomic rates for the same atomic potential as in Eq. (5) but without the periodic continuation. It should be noted that when modeling the ionization by atomic rate equations it is commonly assumed that the electrons leave the atom immediately after they are excited to a free-electron state, thereby disregarding Pauli blocking effects. Note that the Markovian generation rate [Eq. (12)] accounts for Pauli blocking. The most striking difference between calculations based on atomic rates and the results found in Fig. 2(b) for Markovian rates is that when taking the pulse length as the unit of time, the time traces of the free-electron occupation do not depend on the pulse length τ, i.e., changing the pulse length while keeping the total photon number fixed leads only to a rescaling of the time axis. We thus obtain a universal curve for all τ that is plotted in Fig. 6(a).
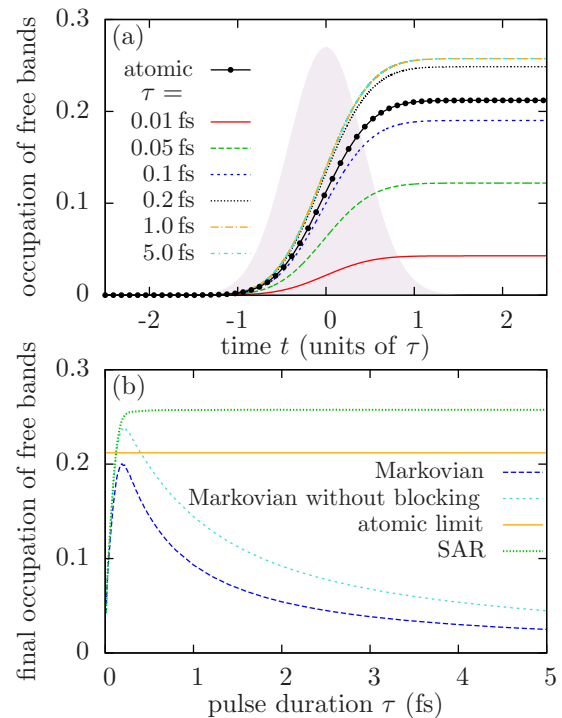
FIG. 6. (Color online) (a) Ionization dynamics for the same conditions as in Fig. 2 but calculated for atomic rates and the spectrally averaged rates (SAR) introduced in the text. Using the pulse length τ as the unit of time, the pulse shape is independent of τ and shown in the background. (b) Comparison of the final values of the free-electron occupations after the pulse obtained from different rate equation approaches as indicated in the legend.

This has to be expected for a model with one-photon absorption cross sections that disregard the blocking and the spectral properties of the pulse, because in this case a fixed percentage of electrons occupying bound states is transferred to free-electron states. Changing the pulse duration while keeping the total intensity fixed just redistributes the transfer differently over the total time of excitation. When in addition the same pulse shape is used in all cases, rescaling the time axis leads to identical curves for the free-electron occupations for all pulse durations.

Evaluation of the cross sections at the central frequency of the pulse according to Eq. (A1) ignores the finite spread of frequencies that is present in any pulse of finite duration. A simple way to account for this effect within the rate equation approach has been suggested in Ref. [32], where the atomic rates in Eq. (A1) have been replaced by their average over the excess energy weighted with the spectral intensity distribution of the pulse. In Ref. [32] this procedure has been applied to an excitation with incoherent radiation where there is not necessarily a connection between the spectral width and the duration of the pulse. In contrast, we are dealing here with Fourier-limited pulses and thus this effect can lead to a dependence of the ionization on the pulse duration. Indeed, following the suggestion of Ref. [32], time traces of the free-electron occupation for different pulse durations do not merely differ by a rescaling of the time axis. However, in our case the difference turns out to be marginal and is therefore not shown. The averaging of the rates has only little impact on the results, mainly because the product $D_{\mathrm{atomic}}(\hbar\omega_{\mathrm{ex}})\,|\langle\psi_i|H_{\mathrm{field}}|\psi_f\rangle|^2$ varies only weakly with the excess energy $\hbar\omega_{\mathrm{ex}}$. It is tempting to think that the averaging recipe can be improved by replacing in Eq. (A1) this product with the corresponding product $D_{\mathrm{crystal}}(\hbar\omega_{\mathrm{ex}})|\langle\psi_{nk\sigma}|H_{\mathrm{field}}|\psi_{jk\sigma}\rangle|^2$ for our crystal model and then performing the average over the pulse spectrum. We shall refer to the thus-modified rates in the following as *spectrally averaged rates* (SAR). Indeed, $D_{\mathrm{crystal}}(\hbar\omega_{\mathrm{ex}})|\langle\psi_{nk\sigma}|H_{\mathrm{field}}|\psi_{jk\sigma}\rangle|^2$ exhibits a more pronounced dependence on $\hbar\omega_{\mathrm{ex}}$, as $D_{\mathrm{crystal}}(\hbar\omega_{\mathrm{ex}})$ changes noticeably near the band edges. Also $|\langle\psi_{nk\sigma}|H_{\mathrm{field}}|\psi_{jk\sigma}\rangle|^2$ may vary significantly with k, as follows from Fig. 1. As is seen from Fig. 6(a), the time trace of the free-electron occupation now depends noticeably on τ. However, this dependence is different from that obtained by the full theory in Fig. 2(a) or by the Markovian limit in Fig. 2(b). It should be noted that replacing the rate by its average over the pulse spectrum is not the same as using rates that depend explicitly on the spectral distribution of the pulse as the Markovian rates in Eq. (12). In fact, the SAR result can be obtained as a limiting case from the Markovian rate approach when it is assumed that the occupation densities

ρ_{nn} do not change significantly within a given band and when Pauli blocking can be neglected. These assumptions are justified, e.g., if the pulse spectrum is broad and structureless and if the product $D_{\mathrm{crystal}}(\hbar\omega_{\mathrm{ex}})|\langle\psi_{nk\sigma}|H_{\mathrm{field}}|\psi_{jk\sigma}\rangle|^2$ can be well approximated by its average. In addition, saturation effects should be small. In fact, for the shortest pulses considered here, the results of the Markovian and the SAR limit are found to be also quantitatively similar. In both approaches, for rising τ there is a maximum of the final free-state occupation, but the subsequent drop that follows the maximum is much less pronounced in the SAR limit. This is most easily seen in Fig. 6(b), where the final values of the free-electron occupation after the pulse are plotted for different rate equation approaches.

As discussed before, one reason for the drop is that an increasing τ makes the pulse spectrum narrow and less excitation falls in the region of high density of states near the band edge. This argument holds, however, in the same way for both the Markovian and the SAR approach. Accounting for rates that explicitly depend on the excess energy leads, for spectrally sharp pulses, to a further concentration of the excitation within a band and to narrower k distributions (not shown), as in a calculation based on a pulse spectrum averaged rate. The consequence is a larger drop of the final free-state occupation in the Markovian case, which is much closer to the outcome of the full quantum-mechanical theory as in the SAR result.

In order to estimate the influence of Pauli blocking effects, we have also performed calculations with Markovian rates where the Pauli blocking is switched off by disregarding the final-state occupation in Eq. (12). The comparison between Markovian simulations with and without Pauli blocking in Fig. 6(b) reveals that the resulting effect on the ionization is quantitatively way too small to explain the large overestimation of the ionization by the atomic rates and the SAR approach, which both disregard the blocking.

Finally, it is interesting to note by comparing all the curves in Fig. 6(b) that for very short pulses a similar ionization is predicted for all levels of the theory, except for the atomic rate approach, which unlike all other approaches, gives a value independent of τ. In particular, in this limit the SAR model also works quite well, which explains to some extent why in many cases this model has given reasonable results for broadband excitations that were not Fourier limited. What matters here is that broadband excitations lead to smooth distributions of the free-electron occupations, which justifies the averaging procedure involved in the SAR limit.

---

[1] V. Ayvazyan, N. Baboi, J. Bähr, V. Balandin, B. Beutner, A. Brandt, I. Bohnet, A. Bolzmann, R. Brinkmann, O. I. Brovko *et al.*, Eur. Phys. J. D **37**, 297 (2006).

[2] P. Emma, R. Akre, J. Arthur, R. Bionta, C. Bostedt, J. Bozek, A. Brachmann, P. Bucksbaum, R. Coffee, F.-J. Decker *et al.*, Nat. Photonics **4**, 641 (2010).

[3] T. Ishikawa, H. Aoyagi, T. Asaka, Y. Asano, N. Azumi, T. Bizen, H. Ego, K. Fukami, T. Fukui, Y. Furukawa *et al.*, Nat. Photonics **6**, 540 (2012).

[4] E. Allaria, R. Appio, L. Badano, W. A. Barletta, S. Bassanese, S. G. Biedron, A. Borga, E. Busetto, D. Castronovo, P. Cinquegrana *et al.*, Nat. Photonics **6**, 699 (2012).

[5] R. R. Fäustlin, T. Bornath, T. Döppner, S. Düsterer, E. Förster, C. Fortmann, S. H. Glenzer, S. Göde, G. Gregori, R. Irsig *et al.*, Phys. Rev. Lett. **104**, 125002 (2010).

[6] B. Rudek, S.-K. Son, L. Foucar, S. W. Epp, B. Erk, R. Hartmann, M. Adolph, R. Andritschke, A. Aquila, N. Berrah *et al.*, Nat. Photonics **6**, 858 (2012).

[7] S.-K. Son, H. N. Chapman, and R. Santra, Phys. Rev. Lett. **107**, 218102 (2011).

[8] B. Schütte, S. Bauch, U. Frühling, M. Wieland, M. Gensch, E. Plönjes, T. Gaumnitz, A. Azima, M. Bonitz, and M. Drescher, Phys. Rev. Lett. **108**, 253003 (2012).

[9] S. Bauch and M. Bonitz, Phys. Rev. A **85**, 053416 (2012).

[10] B. Rudek, D. Rolles, S.-K. Son, L. Foucar, B. Erk, S. Epp, R. Boll, D. Anielski, C. Bostedt, S. Schorb *et al.*, Phys. Rev. A **87**, 023413 (2013).

[11] G. Doumy, C. Roedig, S.-K. Son, C. I. Blaga, A. D. DiChiara, R. Santra, N. Berrah, C. Bostedt, J. D. Bozek, P. H. Bucksbaum *et al.*, Phys. Rev. Lett. **106**, 083002 (2011).

[12] S. M. Vinko, O. Ciricosta, B. I. Cho, K. Engelhorn, H.-K. Chung, C. R. D. Brown, T. Burian, J. Chalupský, R. W. Falcone, C. Graves *et al.*, Nature (London) **482**, 59 (2012).

[13] R. Neutze, R. Wouts, D. van der Spoel, E. Weckert, and J. Hajdu, Nature (London) **406**, 752 (2000).

[14] N. Rohringer and R. Santra, Phys. Rev. A **76**, 033416 (2007).

[15] E. L. Saldin, E. A. Schneidmiller, and M. V. Yurkov, New J. Phys. **12**, 035010 (2010).

[16] I. Grguraš, A. R. Maier, C. Behrens, T. Mazza, T. J. Kelly, P. Radcliffe, S. Düsterer, A. K. Kazansky, N. M. Kabachnik, T. Tschentscher *et al.*, Nat. Photonics **6**, 852 (2012).

[17] B. Kaiser, A. Vagov, V. M. Axt, and U. Pietsch, Phys. Rev. A **84**, 043431 (2011).

[18] B. Kaiser, A. Brand, M. Glässl, A. Vagov, V. M. Axt, and U. Pietsch, New J. Phys. **15**, 093016 (2013).

[19] E. P. Kanter, B. Krässig, Y. Li, A. M. March, P. Ho, N. Rohringer, R. Santra, S. H. Southworth, L. F. DiMauro, G. Doumy *et al.*, Phys. Rev. Lett. **107**, 233001 (2011).

[20] N. Rohringer and R. Santra, Phys. Rev. A **77**, 053404 (2008).

[21] N. Rohringer and R. Santra, Phys. Rev. A **86**, 043434 (2012).

[22] B. W. J. McNeil and N. R. Thompson, Nat. Photonics **4**, 814 (2010).

[23] J. N. Galayda, J. Arthur, D. F. Ratner, and W. E. White, J. Opt. Soc. Am. B-Opt. Phys. **27**, B106 (2010).

[24] E. Allaria, C. Callegari, D. Cocco, W. M. Fawley, M. Kiskinova, C. Masciovecchio, and F. Parmigiani, New J. Phys. **12**, 075002 (2010).

[25] J. Amann, W. Berg, V. Blank, F.-J. Decker, Y. Ding, P. Emma, Y. Feng, J. Frisch, D. Fritz, J. Hastings *et al.*, Nat. Photonics **6**, 693 (2012).

[26] S.-K. Son, L. Young, and R. Santra, Phys. Rev. A **83**, 033402 (2011).

[27] H.-K. Chung, M. H. Chen, and R. W. Lee, High Energy Density Phys. **3**, 57 (2007).

[28] D. N. Fittinghoff, P. R. Bolton, B. Chang, and K. C. Kulander, Phys. Rev. Lett. **69**, 2642 (1992).

[29] B. Walker, B. Sheehy, L. F. DiMauro, P. Agostini, K. J. Schafer, and K. C. Kulander, Phys. Rev. Lett. **73**, 1227 (1994).

[30] D. G. Lappas and R. van Leeuwen, J. Phys. B: At. Mol. Opt. Phys. **31**, L249 (1998).

[31] Y. Ding, A. Brachmann, F.-J. Decker, D. Dowell, P. Emma, J. Frisch, S. Gilevich, G. Hays, P. Hering, Z. Huang *et al.*, Phys. Rev. Lett. **102**, 254801 (2009).

[32] A. Sytcheva, S. Pabst, S.-K. Son, and R. Santra, Phys. Rev. A **85**, 023414 (2012).

[33] H. Le Rouzo, Am. J. Phys. **73**, 962 (2005).

[34] Note that the work function essentially provides a finite energy offset of a few electronvolts, which is not of great importance on the energy scales that we are interested in here.

[35] C. Ruiz, L. Plaja, and L. Roso, Phys. Rev. Lett. **94**, 063002 (2005).

[36] F. Rossi and T. Kuhn, Rev. Mod. Phys. **74**, 895 (2002).

[37] L. Young, E. P. Kanter, B. Kraessig, Y. Li, A. M. March, S. T. Pratt, R. Santra, S. H. Southworth, N. Rohringer, L. F. DiMauro *et al.*, Nature (London) **466**, 56 (2010).

[38] M. Hoener, L. Fang, O. Kornilov, O. Gessner, S. T. Pratt, M. Gühr, E. P. Kanter, C. Blaga, C. Bostedt, J. D. Bozek *et al.*, Phys. Rev. Lett. **104**, 253002 (2010).

[39] M. Beye, S. Schreck, F. Sorgenfrei, C. Trabant, N. Pontius, C. Schüßler-Langeheine, W. Wurth, and A. Föhlisch, Nature (London) **501**, 191 (2013).

[40] T. Sako, J. Adachi, A. Yagishita, M. Yabashi, T. Tanaka, M. Nagasono, and T. Ishikawa, Phys. Rev. A **84**, 053419 (2011).

[41] T. Sato, A. Iwasaki, K. Ishibashi, T. Okino, K. Yamanouchi, J. Adachi, A. Yagishita, H. Yazawa, F. Kannari, M. Aoyma *et al.*, J. Opt. Soc. Am. B: Opt. Phys. **44**, 161001 (2011).

[42] Here, only the part of H_{field} that is linear in the vector potential is used.